Optical Engineering

SPIEDigitalLibrary.org/oe

Measuring of temperatures of a candle flame using four multidirectional point-diffraction interferometers

Juan C. Aguilar
Luis Raul Berriel-Valdos
Jose Felix Aguilar

Measuring of temperatures of a candle flame using four multidirectional point-diffraction interferometers

Juan C. Aguilar
Luis Raul Berriel-Valdos
Jose Felix Aguilar
Instituto Nacional de Astrofísica Óptica y Electrónica
Luis E. Erro No. 1, Tonantzintla
Puebla, C. P. 72840 México
E-mail: juandspcf@gmail.com

Abstract. An optical system formed by four point-diffraction interferometers is used for measuring the temperature distribution of a candle flame. It is assumed that the phase can be expressed in terms of the Radon transform, and it is processed with a tomographic iterative algorithm to obtain the temperatures. The interferograms show the asymmetry of the candle flame, justifying the use of a tomographic iterative algorithm instead of the Abel inversion. The resulting temperature distribution verifies the usefulness of the proposed method. [DOI: 10.1117/1.OE.52.10.104103]

Subject terms: tomography; inverse problems; interferogram processing; point-diffraction interferometer.

Paper 131089P received Jul. 18, 2013; revised manuscript received Sep. 23, 2013; accepted for publication Sep. 23, 2013; published online Oct. 10, 2013.

1 Introduction

Most of the optical setups for measuring the temperatures of flames are based on holographic systems or on standard interferometers like Mach-Zehnder and Twyman-Green.[1] Goldmeer et al.[2] presented an implementation with a point-diffraction interferometer (PDI), but the measurement was limited by the characteristics of the commercial system they used (Smartt Interferometer, Coherent Inc., Santa Clara, California). One of the constraints, among others, was, for example, the extension in diameter of the analyzed flame, which was ∼0.5 cm. Despite the simplicity of the PDI, to our knowledge, further works have not been reported yet. The other issue is the lack of symmetry of the flame; most of the works deal with symmetric flames, where temperatures can be easily computed by Abel inversion technique. However, in a candle flame, the wick, the quality of the wax, and the way the heat melts the top of the massive solid fuel determines the distribution of temperatures and this can be asymmetric. So it is advisable to take more projections for a better estimation of the temperatures. Wei et al.[3] used three lateral shearing interferometers and recovered the temperatures of a diffused ethylene flame with two tomographic algorithms, filtered back projection (FBP) and Abel inversion. If the number of projections of an asymmetric object is dense, the best algorithm is FBP, but when the number of projections is small, the tomographic iterative algorithms work better than FBP as it has been shown by Ko and Kihm.[4]

In this work, we present an optical system that is easy to implement and formed by four PDIs, for measuring the temperatures distribution of a candle flame. Due to the small number of projections and the asymmetry present in the interferograms of the flame, the computation of temperature is performed by a tomographic iterative algebraic algorithm (Kaczmarz). The recovery of the phase is made numerically with the method of Kreis.[5] This uses the Fourier transform and it is adequate for interferograms with few fringes. In Sec. 2, we present the theory on which our proposed technique is based; then in Sec. 3, the experiment is described, and the results are presented in Sec. 4. Finally, remarks and conclusions are in Sec. 5.

2 Theory

One of the most common ways to measure the temperatures of phase objects like gases, deduced from the refractive index, is to use the Gladstone-Dale equation,

$$\frac{n-1}{\rho} = K(\lambda), \tag{1}$$

where n is the refraction index of the object, ρ is the density, and K is known as the Gladstone-Dale constant, which is a property of the gas and slightly dependent on the wavelength (λ).[1] From Eq. (1), the relation between the temperatures and the refraction index is given by

$$T = \left[\frac{1}{T_0} - \frac{(n_0 - n)R}{K(\lambda)MP}\right]^{-1}, \tag{2}$$

where n_0 is the refractive index of the environment, M is the molecular weight of the gas, P and T are the gas-phase pressure and temperature, respectively, R is the universal gas constant, and T_0 is the reference temperature. The quantity $(n - n_0)$ in Eq. (2), which is also represented by Δn, is found by the integral expressing the optical path difference $\Delta\phi$ between the refractive index of the environment and that corresponding to the phase object.

$$\Delta\phi = \int [n_0 - n(x, y, z)]\mathrm{d}s = \int \Delta n \,\mathrm{d}s. \tag{3}$$

But if the refraction on the rays through the phase object is assumed small, Eq. (3) can be expressed as

$$\Delta\phi = N\lambda = \int [n_0 - n(x, z)]\mathrm{d}z = \int \Delta n \,\mathrm{d}z, \tag{4}$$

where N is the order of interference and z is the axial coordinate. Equation (4) means that when a plane wave has

passed through, for example, a flame, its refraction is negligible, and we can assume rays traveling in a direction parallel to the axis as is shown in Fig. 1.

The wave front $\Delta\phi$ under this approximation is easily measured with a PDI.[6] The layout of a PDI system is shown in Fig. 2. The wave front associated with the object beam is focused on a pinhole in the semiabsorbing thin film deposited on the glass plate. The object beam passes through the plate and diverges, while a reference wave front beam is generated from the pinhole. These two beams interfere in the far field. The number of fringes in the corresponding interferogram can be increased as the PDI plate is tilted; however, an inconvenient reduction of contrast comes as well. Equation (4) has another meaning, as is shown by Deans;[7] it can be interpreted as the Radon transform of Δn at the angle $\theta = 0$ deg. The general expression for the Radon transform of Δn is given by

$$\Re(t,\theta) = \int_{-\infty}^{\infty}\int_{-\infty}^{\infty}[n_0 - n(x,z)]\delta(t - z\cos\theta - x\sin\theta)\mathrm{d}x\mathrm{d}z, \tag{5}$$

where $\Re(t,\theta)$ denotes the optical path difference, taken from the interferogram on a given θ angle and a height y, with t as its axis and δ as the Dirac delta function. In the case of many views, Δn can be recovered by the use of the FBP algorithm. Otherwise, if we have only a small number of views, iterative algorithms will work better.

In iterative algorithms, the quantity f (Δn for the experiment) that we try to recover is approximated by a function f_a, which, at the same time, is formed as a sum of basis functions B in the following form:

$$f_a = \sum_{k=1}^{M} c_k B_k(x,z). \tag{6}$$

Here, B can be an interpolating basis function as the bicubic function or a noninterpolating one as the cubic spline function, and we decided to use the bicubic basis function, as its approximation quality is enough for getting a good representation of Δn. When B is interpolating, the coefficients c_k correspond to discrete values of f within a square array of size $\Lambda \times \Lambda = M$ elements. The Radon transform of f_a is the sum of the Radon transforms for each B_k, without any change on the coefficients c_k. The Radon transform can be envisioned as a ray that integrates to f_a only at points (x,z) that fulfills the line equation $t_i - z\cos\theta_j - x\sin\theta_j = 0$ as is shown in Fig. 3. In Fig. 3(a), we show an example of some basis functions that form f_a, and in Fig. 3(b) is shown a ray that integrates some of the basis functions according to a line equation. For any duple (t_i,θ_j), we have an equation given by

$$c_1 w_1\{t_i,\theta_j\} + c_2 w_2\{t_i,\theta_j\} + c_3 w_3\{t_i,\theta_j\} + \ldots + c_M w_M\{t_i,\theta_j\} = p\{t_i,\theta_j\}, \tag{7}$$

where $w_k\{t_i,\theta_j\}$ represents the contribution of the Radon transforms of B_k performed for the ray R_i and $p\{t_i,\theta_j\}$ is the sum of all those contributions. All the resulting equations are arranged in a matrix equation as follows:

$$\mathbf{WC} = \mathbf{P}. \tag{8}$$

Here, $\mathbf{W}$ is the matrix of $L \times M$ formed by all the contributions $w_k\{t_i,\theta_j\}$, $\mathbf{C}$ is the vector with components $\{c_1, c_2, c_3, \ldots, c_M\}$, and the vector $\mathbf{P}$ of $L \times 1$ elements contains all ray integrals values, i.e., $\mathbf{P}$ is the experimental data. If the basis function $B(x,z)$ is separable and even, its Radon transform can be expressed as

$$p_\theta(t) = p_{\theta,t}\{B(x,z)\} = \int\int B(x)B(z)\delta(t - z\cos\theta - x\sin\theta)\mathrm{d}z\mathrm{d}x, \tag{9}$$

$$= \frac{1}{|\sin\theta||\cos\theta|}\int B\left(\frac{\alpha}{|\sin\theta|}\right)B\left(\frac{t-\alpha}{|\cos\theta|}\right)\mathrm{d}\alpha, \tag{10}$$

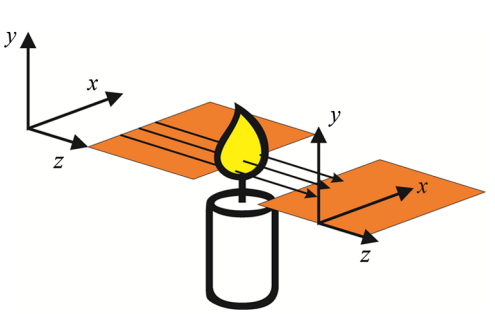

Fig. 1 One of the planes defining the projections.

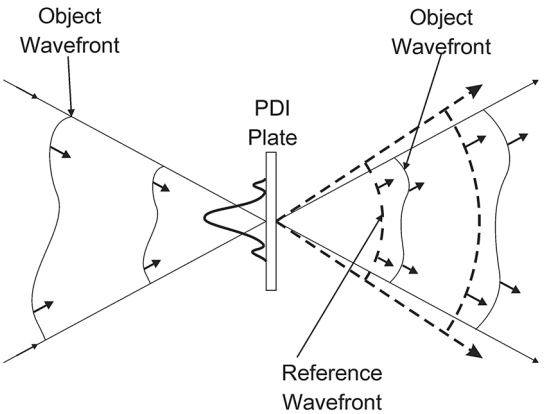

Fig. 2 Schematic diagram of the point-diffraction interferometer, describing the work of the coated plate with a pinhole in the center for generating two wave fronts.

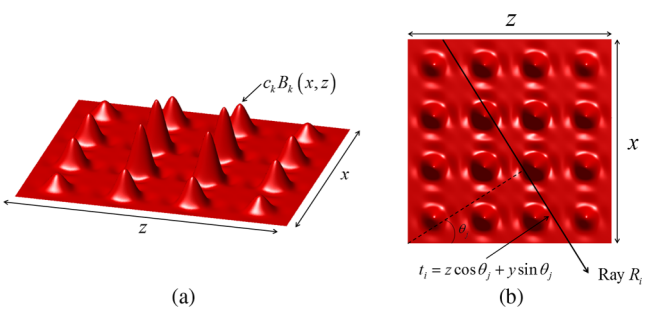

Fig. 3 Radon transform space. (a) Representation of f_a by a set of basis functions. (b) Coordinates of integration of the Radon.

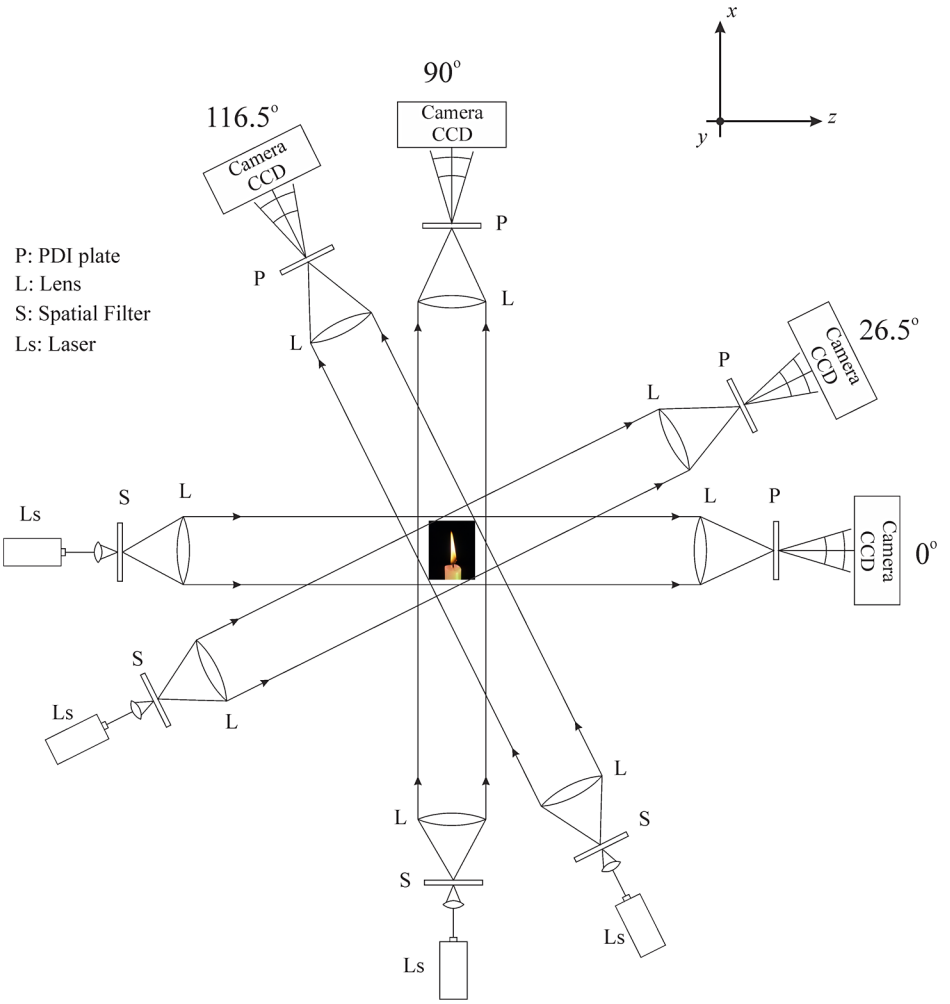

Fig. 4 Experimental setup presenting the four interferometers.

$$= \frac{1}{|\sin\theta||\cos\theta|} B\left(\frac{t}{|\sin\theta|}\right) * B\left(\frac{t}{|\cos\theta|}\right), \quad \text{for every angle, except } \theta = [0,180,90,270] \tag{11}$$

where * denotes a convolution operation and $\alpha = x|\sin\theta|$. Equation (11) means that the Radon transform of a separable basis function can be easily computed with a fast Fourier transform algorithm or have an exact representation of the Radon transform if the basis function is polynomial, as is in our case. We use an algebraic reconstruction technique to solve Eq. (8), the Kaczmarz iterative algorithm, which is expressed in the following form:[8,9]

$$\mathbf{C}^n = \mathbf{C}^{n-1} + \xi \frac{(\mathbf{P}_n - \mathbf{W}_{n,*}\mathbf{C}^{n-1})}{(\mathbf{W}_{n,*})(\mathbf{W}_{n,*})^T} (\mathbf{W}_{n,*})^T, \tag{12}$$

where ξ is a relaxing parameter with $0 < \xi < 2$, n letter is the iteration number, and $\mathbf{W}_n$,* denotes the n'th row of matrix $\mathbf{W}$. If the equations system (8) has a unique solution, then $\mathbf{C}^n$ will converge to this solution. If the system of equations has many solutions, then $\mathbf{C}^n$ will converge to the solution that is closest to the point $\mathbf{C}^0$, which is a solution of minimum 2-norm. If we start with $\mathbf{C}^0 = 0$, we will obtain a minimum-length solution. If there is no exact solution of the system of equations, then Eq. (10) will fail to converge, but it will typically bounce around near an approximate solution.[8,9]

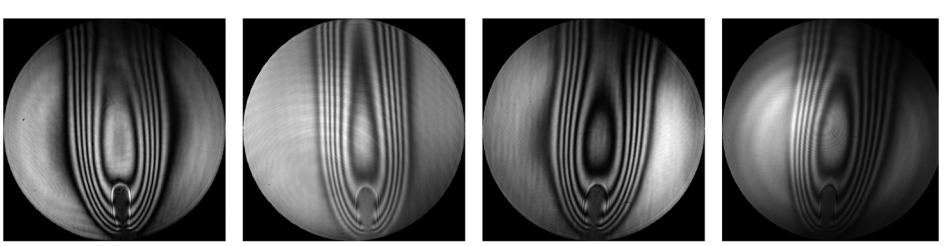

Fig. 5 Resulting interferograms from the optical setup in Fig. 4.

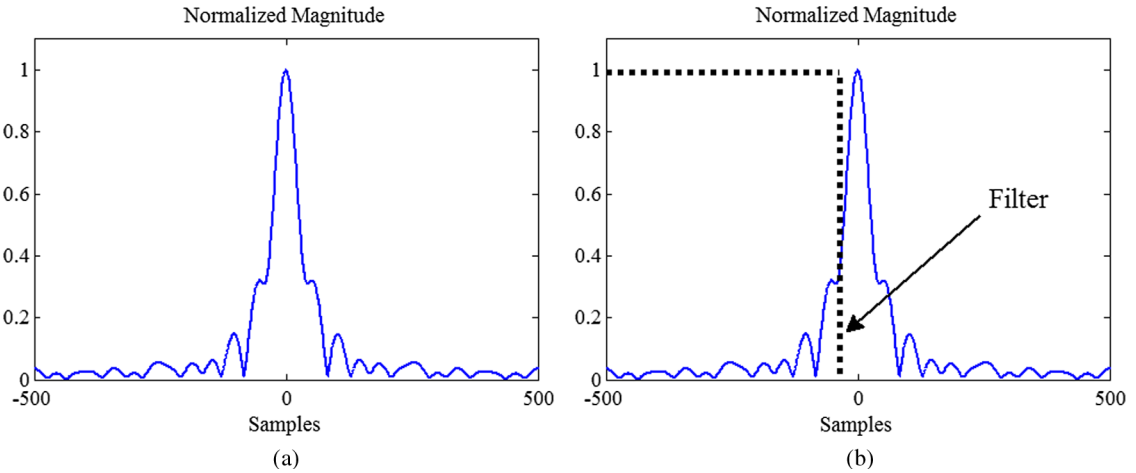

Fig. 6 Fourier transform of $I(x)$. (a) Normalized magnitude distribution. (b) Filtering region.

However, even though Eq. (8) has an exact solution, if the vector **P** includes the noise, there will be a behavior called semiconvergence.[9] At the beginning, $\mathbf{C}^n$ converges to the exact solution, but after certain number of iterations, $\mathbf{C}^n$ begins to capture information of the noise in **P**. So, in order to control the noise level, it is necessary to apply a filtering in each iteration. The parameter ξ also controls the semiconvergence; for values about $\xi \geq 1$, the convergence will grow quickly but the noise also is amplified fast. When $\xi \leq 0.1$, the convergence is slow and the noise is

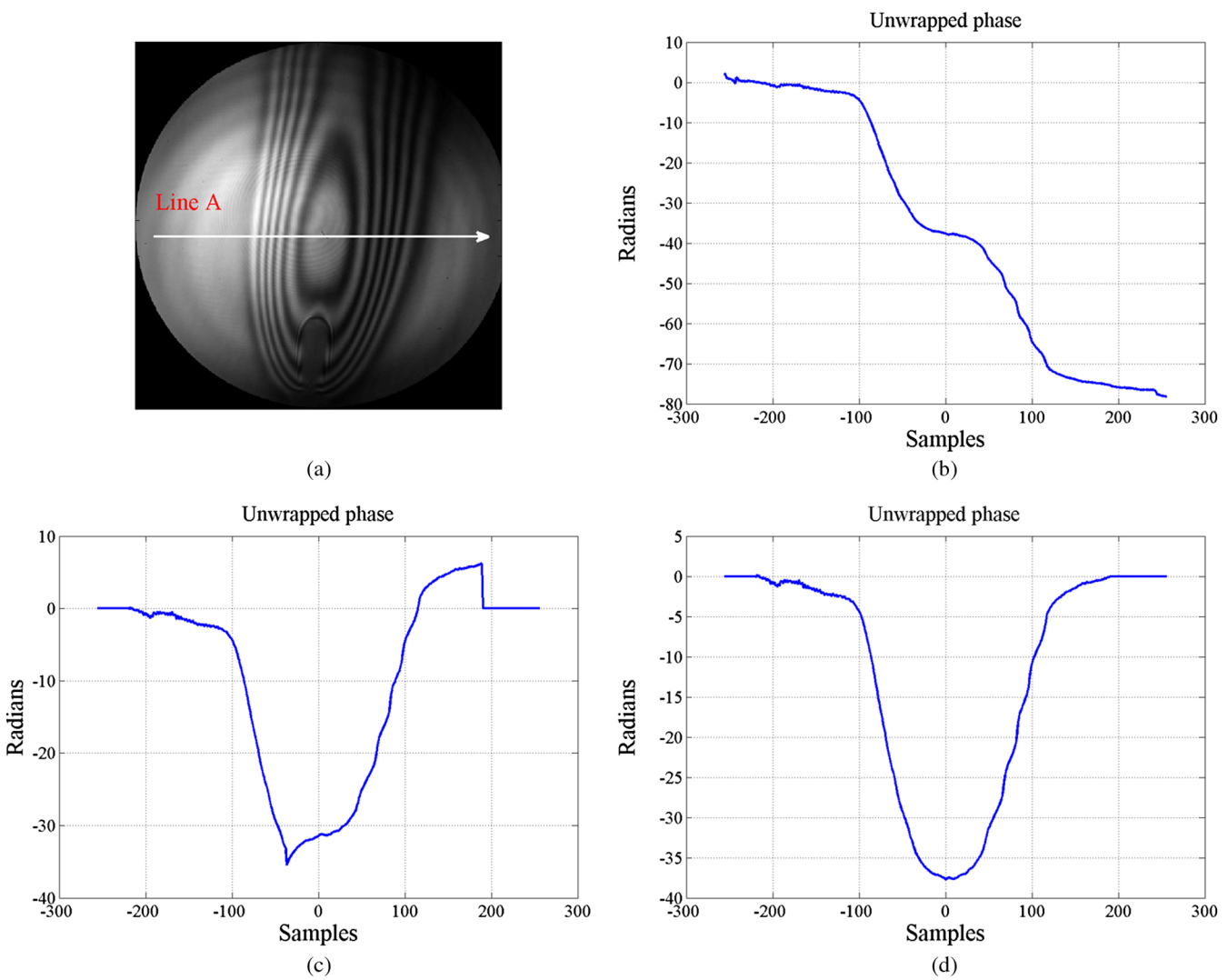

Fig. 7 Phase determination of an interferogram of a candle flame. (a) Interferogram used. (b) Phase with sign changed. (c) Wrong reversed point. (d) Correct reversed point.

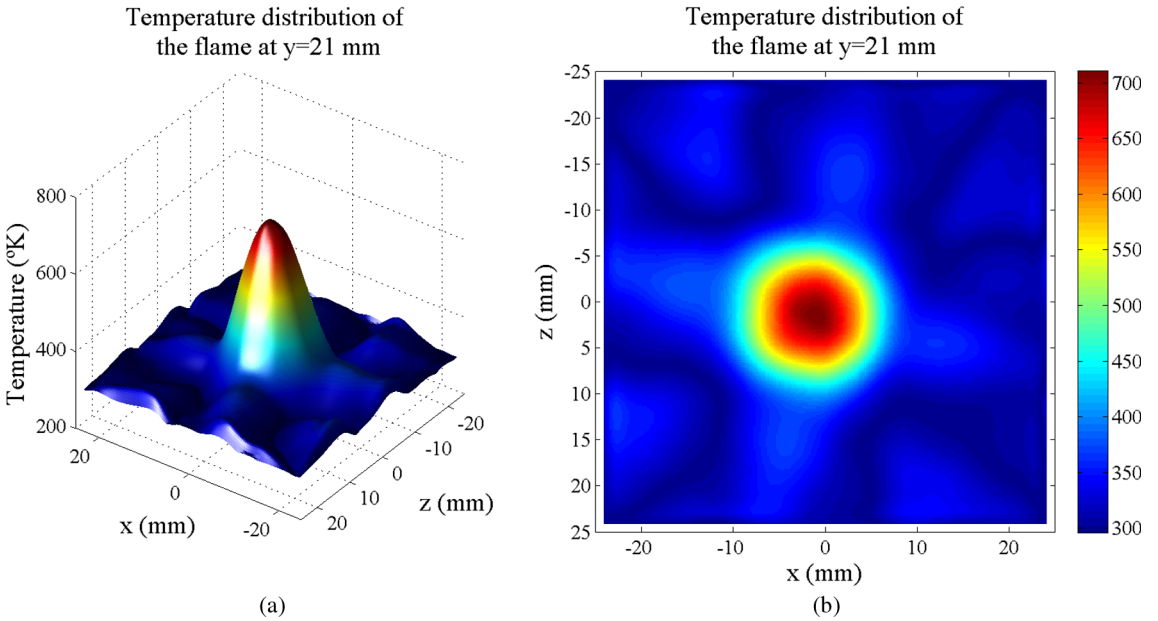

Fig. 8 Tomographic reconstruction at $y = 21$ mm related to $\mathbf{C}^0 = 0$, unconstrained $\mathbf{C}^n$, and $\xi = 0.01$. (a) Surface representation of the temperatures distribution. (b) Level curves representation of the temperatures distribution.

not so amplified.[9] In this work, $\xi = 0.01$ is selected at the expenses of a very slow convergence; still, in the final iterations, we will find a solution without many effects of the noise.

3 Description of the Experiment

In order to measure the refractive index, we have chosen the directions of the four PDIs distributed at 0, 90, 26.5, and 116.5 deg, as is shown in Fig. 4. The limited size of the optical bench, where the optical setup was located, imposes the selection of these particular angles. Lenses L1 and L2 in each interferometer are 30 cm of focal length with diameter $D = 4.6$ cm. The illumination is a collimated laser beam of 35 mW power and a wavelength of 532 nm. The phase object is placed at the intersection of all the four plane waves to perform the tomography. The detected interferograms for a candle flame of ~2.4 cm of width are shown in Fig. 5 wherein we can observe they have a suitable contrast for processing, and also, the aberrations of the lenses do not perturb the interferograms significantly. One can suppose a radial symmetry of the candle flame from the interferogram at 26.5 deg, but the other interferograms showed the opposite; therefore, it is not recommendable to use the Abel inversion algorithm.

The phase retrieval for interferograms in infinite mode with few fringes, is usually made with the fitting of a function over the order numbers N.[1] The Fourier transform is traditionally applicable when the interferogram has an enough density of fringes, but with the method of Kreis,[5] this can be made with fewer fringes. We computed the discrete Fourier transform of the interferogram at a given height. That part of the interferogram can be described with three components.

$$\begin{aligned} I(x) &= a(x) + b(x)\cos[\phi(x)], \\ &= a(x) + c(x) + c^*(x), \\ c(x) &= \frac{1}{2} b(x) e^{j\phi(x)}, \end{aligned} \tag{13}$$

where $a(x)$ is the irradiance sum of the object and reference beams, $b(x)$ are multiplicative effects over the interferogram, and $\phi(x)$ is the phase change. The Fourier transform of $I(x)$ will be even-symmetric. This is shown in Fig. 6(a). If the Fourier transform is filtered in Eq. (11), as is shown in Fig. 6(b), the recovered phase unwrapped $\phi^{(r)}(x)$ has the property to present a region where the original phase $\phi(x)$ is reversed; this is shown in Fig. 7(b). However, that feature can be overcome inverting the wrapped phase after of a determined point η. This process is illustrated in Fig. 7. Figure 7(a) shows the selected interferogram, and the phase is estimated over the line A. If we select a wrong η, the unwrapped phase will have a kind of discontinuity as shown in Fig. 7(c). However, the phase associated with the flame is a smooth function, so we must not have discontinuities after the unwrapping process; therefore, we can set a criterion of continuity: the approximate reversing point that

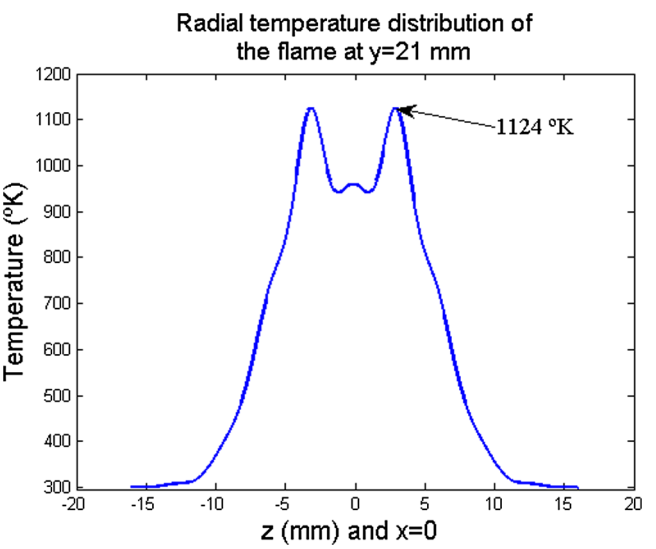

Fig. 9 Temperature distribution based on Abel inversion.

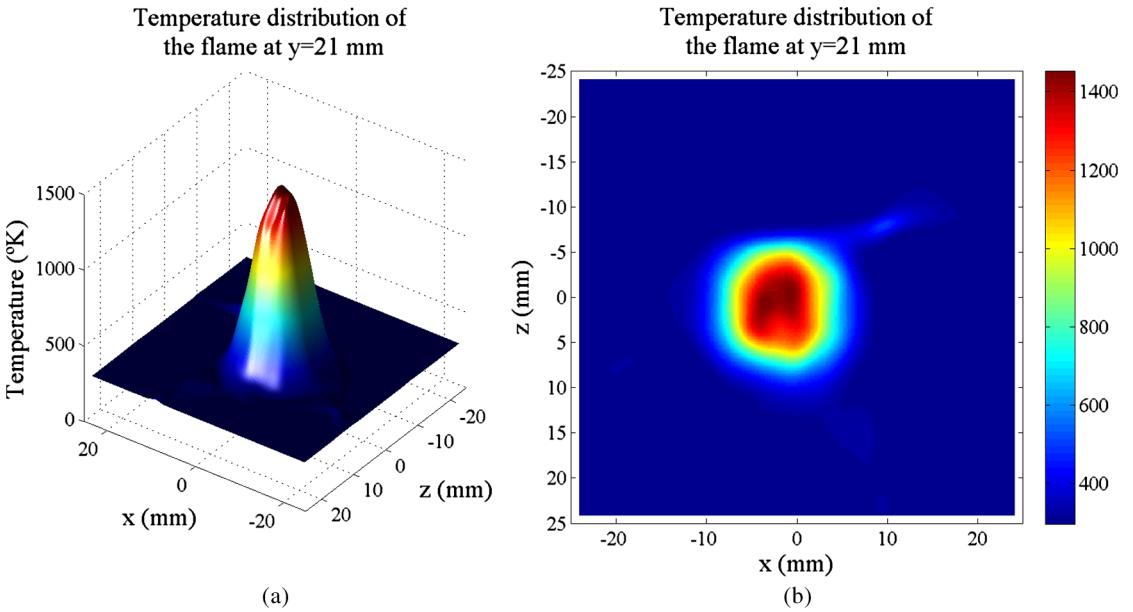

Fig. 10 Tomographic reconstruction at $y = 21$ mm related to $\mathbf{C}^0 =$ Abel solution, $\mathbf{C}^n < 0$, and $\xi = 0.01$. (a) Surface representation of the temperatures distribution. (b) Level curves representation of the temperatures distribution.

produces the smoothest phase function will be chosen as the point of inversion. Figure 7(c) shows a wrong reversing point, and Fig. 7(d) shows a reversing point that provides a smoother phase function $\phi^{(r)}(x)$.

We used CCD cameras of 4592×3056 pixels for the capture of the interferograms. However, its Fourier transform will be undersampled because of the property that a big support at the spatial domain corresponds to a small support in the frequency domain. The chosen cut-off frequency also determines how $\phi^{(r)}(x)$ resembles the original phase function $\phi(x)$. If the cut-off frequency is a high value in any direction with respect to the origin, we lose information about $\phi(x)$, so it is recommendable to select the cut-off frequency near to the origin, as, for example, that shown in Fig. 6(b). In order to realize the process described above, another recommendation is to reduce the size of the interferogram and make padding with zeros in the rest of the field; this is called the zero-padding technique. The Fourier transform will have a better sampling, and consequently, it is possible to choose a cut-off frequency with finer steps.

4 Results

We tested two different possibilities of inputs for the Kaczmarz algorithm as it will be seen later. Once $\mathbf{C}^n$ is computed, a low-pass filtering is applied on it, so the noise in high frequencies is diminished. However, the result is not used as an update of Eq. (10), but is used for computing the temperatures distribution. The reason underlying that procedure is that we do not want to make a strong modification of $\mathbf{C}^n$ in each iteration. Since the pass-band region of the applied filter is not uniform, there would be the possibility

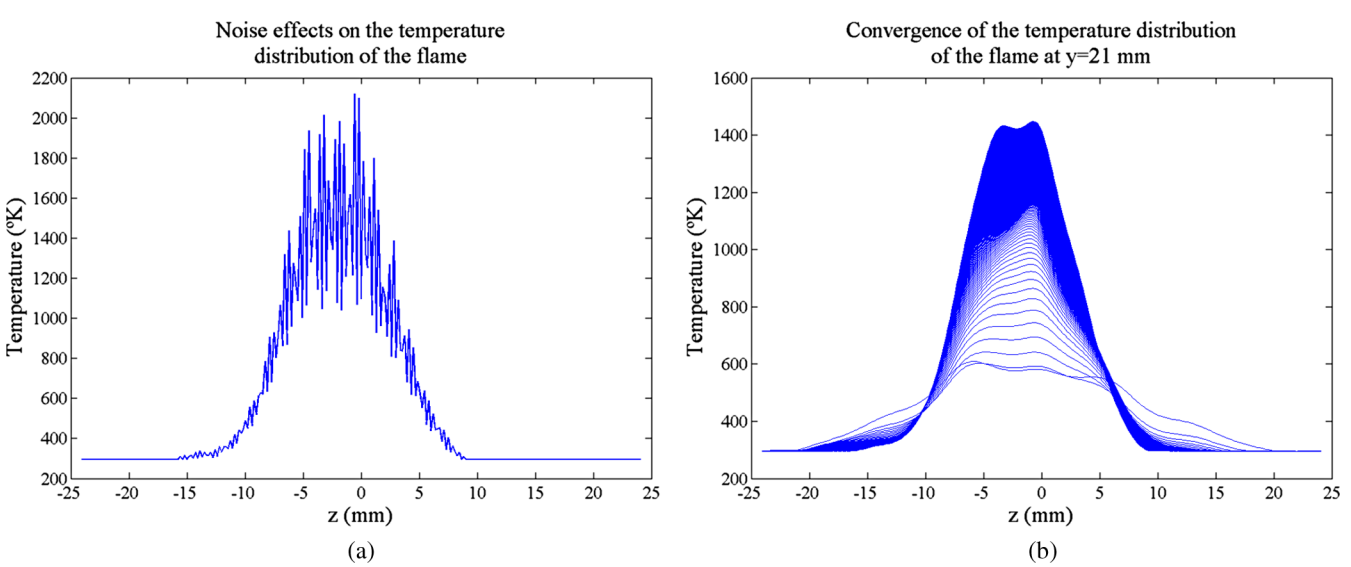

Fig. 11 Noise effects and converge of the temperatures related to $\mathbf{C}^n$. (a) The noise destroys the shape of the temperature distribution. (b) The shape of the temperatures converging after the iterative process.

of modifying important information in $\mathbf{C}^n$. Therefore, for each updated $\mathbf{C}^n$, we might wrongly change its convergence. The iterations are stopped when the corresponding temperatures of the filtered $\mathbf{C}^n$ seem to reach a fixed value. We use the data coming from the interferograms at a height of 21 mm for the following results. The first try is with $\mathbf{C}^0 = 0$, unconstrained $\mathbf{C}^n$, and $\xi = 0.01$, and the results are shown in Fig. 8. The maximum temperature using Eq. (2) is 711°K, but it does not represent a realistic distribution of temperatures because that means that the flame is not hot. For the case of $\mathbf{C}^0$ different than zero, $\mathbf{C}^n < 0$, and $\xi = 0.01$, we choose the Abel inversion solution $\mathbf{C}^A$ as the starting point $\mathbf{C}^0$. $\mathbf{C}^A$ is taken from the interferogram at 116.5 deg at a height of 21 mm [Fig. 7(a)]. The phase of the interferogram is computed at 116.5 deg due to its corresponding radial symmetric temperature distributions, which closely resemble the measure reported in other works.[10] The temperature distribution taking $\mathbf{C}^A$ is shown in Fig. 9.

According to the foregoing, we show the temperature distribution in Fig. 10, wherein the maximum value is 1454°K. The maximal possible temperature of a candle flame is 1673°K.[11,12] Of course, the possibility of reaching this value in our measurements depends on the manufacturing process of the wax and wick. Therefore, the solution shown in Fig. 10 seems physically reliable unlike the result shown in Fig. 8. If the filtering is not applied for $\mathbf{C}^n$, the reconstructed distribution of temperatures is shown in Fig. 11(a), where the severe effects of the noise can be seen. However, using filtering, the computed temperatures reach a limit shape as shown in Fig. 11(b).

5 Remarks and Conclusions

From our results, we can remark that the interferogram so obtained from the PDIs have enough quality to be considered as projections of the candle flame. They are comparable to those obtained with other techniques, such as digital holography, but, in this case, with less complexity required for the optical system.

Since the interferograms are on infinite mode and in order that the projected fringes are those of the flame only, the lenses in the setup have to be well corrected of aberrations.

Since this kind of interferogram has a low density of fringes, we have used the method of Kreis for recovering the phase.

The interferograms show the asymmetry of the candle flame; hence it is not recommendable to use the inverse Abel transform as is commonly done. If we use the Abel solution for each interferogram, the results become different because each interferogram has a different shape. Nevertheless, the Abel solution can be useful as an initial solution to the iterative algorithm, giving an estimate with less error.

The Kaczmarz algorithm shows its usefulness in the recovering of information with few projections, but we must apply a filtering due to the amplification of the noise in each iteration. We also have to use an initial condition different than zero and constrain the iterations to be less than zero. This is with the purpose of having realistic solutions.

So, we can conclude that this is a very simple and accurate technique to measure the temperatures distribution in a candle flame, which can also be applied to other objects with similar geometric and material characteristics.

References

1. C. M. Vest, *Holographic Interferometry*, John Wiley & Sons, New York (1979).
2. J. S. Goldmeer, D. L. Urban, and Z.-G. Yuan, "Measurement of gas-phase temperatures in flames with a point-diffraction interferometer," *Appl. Opt.* **40**(27), 4816–4823 (2001).
3. W. Lv, H.-C. Zhou, and J.-R. Zhu, "Implementation of tridirectional large lateral shearing displacement interferometry in temperature measurement of a diffused ethylene flame," *Appl. Opt.* **50**(21), 3924–3936 (2011).
4. H. S. Ko and K. D. Kihm, "An extended algebraic reconstruction technique (ART) for density gradient projections: laser speckle photographic tomography," *Exp. Fluids* **27**(6), 542–550 (1999).
5. T. Kreis, "Digital holographic interference-phase measurement using the Fourier-transform method," *J. Opt. Soc. Am. A* **3**(6), 847–855 (1986).
6. J. M. Geary, *Introduction to Wavefront Sensors*, SPIE Press, Tutorial Text in Optical Engineering, Bellingham, Washington (1995).
7. S. R. Deans, *The Radon Transform and Some of Its Applications*, Dover Publications, New York (1993).
8. R. C. Aster, B. Borchers, and C. H. Thurber, *Parameter Estimation and Inverse Problems*, Academic Press, San Diego, California (2005).
9. C. Hansen and M. Saxild-Hansen, "AIR tools—a MATLAB package of algebraic iterative reconstruction methods," *J. Comput. Appl. Math.* **236**(8), 2167–2178 (2012).
10. S. Sharma, G. Sheoran, and C. Shakher, "Digital holographic interferometry for measurement of temperature in axisymmetric flames," *Appl. Opt.* **51**(16), 3228–3235 (2012).
11. A. Hamins, M. Bundy, and S. E. Dillon, "Characterization of candle flames," *J. Fire Protect. Eng.* **15**(4), 265–285 (2005).
12. K. Roth, "Alle Jahre wieder: die Chemie der Weihnachtskerze," *Chemie in unserer Zeit* **37**(6), 424–429 (2003).

Biographies and photographs of the author are not available.